American Journal of Life Sciences
2017; 5(1): 11-20
http://www.sciencepublishinggroup.com/j/ajls
doi: 10.11648/j.ajls.20170501.13
ISSN: 2328-5702 (Print); ISSN: 2328-5737 (Online)

Evaluation of the Trivedi Effect®- Energy of Consciousness Energy Healing Treatment on the Physical, Spectral, and Thermal Properties of Zinc Chloride

Mahendra Kumar Trivedi[1], Alice Branton[1], Dahryn Trivedi[1], Gopal Nayak[1], Cathryn Dawn Nykvist[1], Celine Lavelle[1], Daniel Paul Przybylski[1], Dianne Heather Vincent[1], Dorothy Felger[1], Douglas Jay Konersman[1], Elizabeth Ann Feeney[1], Jay Anthony Prague[1], Joanne Lydia Starodub[1], Karan Rasdan[1], Karen Mie Strassman[1], Leonid Soboleff[1], Maire Anne Mayne[1], Mary M. Keesee[1], Padmanabha Narayana Pillai[1], Pamela Clarkson Ansley[1], Ronald David Schmitz[1], Sharyn Marie Sodomora[1], Kalyan Kumar Sethi[2], Parthasarathi Panda[2], Snehasis Jana[2, *]

[1]Trivedi Global, Inc., Henderson, Nevada, USA

[2]Trivedi Science Research Laboratory Pvt. Ltd., Bhopal, Madhya Pradesh, India

Email address:

publication@trivedieffect.com (S. Jana)

[*]Corresponding author

To cite this article:

Mahendra Kumar Trivedi, Alice Branton, Dahryn Trivedi, Gopal Nayak, Cathryn Dawn Nykvist, Celine Lavelle, Daniel Paul Przybylski, Dianne Heather Vincent, Dorothy Felger, Douglas Jay Konersman, Elizabeth Ann Feeney, Jay Anthony Prague, Joanne Lydia Starodub, Karan Rasdan, Karen Mie Strassman, Leonid Soboleff, Maire Anne Mayne, Mary M. Keesee, Padmanabha Narayana Pillai, Pamela Clarkson Ansley, Ronald David Schmitz, Sharyn Marie Sodomora, Kalyan Kumar Sethi, Parthasarathi Panda, Snehasis Jana. Evaluation of the Trivedi Effect®- Energy of Consciousness Energy Healing Treatment on the Physical, Spectral, and Thermal Properties of Zinc Chloride. *American Journal of Life Sciences*. Vol. 5, No. 1, 2017, pp. 11-20. doi: 10.11648/j.ajls.20170501.13

Received: January 31, 2017; **Accepted**: February 14, 2017; **Published**: February 25, 2017

Abstract: Zinc chloride has the importance in pharmaceutical/nutraceutical industries for the prevention and treatment of several diseases. The objective of the current study was to investigate the impact of The Trivedi Effect®-Energy of Consciousness Healing Treatment (Biofield Energy Healing Treatment) on physical, structural, and thermal properties of zinc chloride using PXRD, PSD, FT-IR, UV-vis, TGA, and DSC analysis. Zinc chloride was divided into two parts. One part was denoted as the control without any, while the other part was defined as the Trivedi Effect® Treated sample, which received the Trivedi Effect® Treatment remotely from eighteen renowned Biofield Energy Healers. The PXRD analysis revealed that the crystallite size and relative intensities of the PXRD peaks significantly altered in the treated sample compared with the control sample. The crystallite size of treated sample was decreased by 4.19% compared with the control sample. The particle size at d_{10} and d_{50} of the Biofield Energy Treated sample decreased by 4.72% and 2.70%, respectively compared with the control sample. But, the particle size of the treated sample increased at d_{90} by 0.83 compared with the control sample. Consequently, the surface area was increased by 3.22% in the treated sample compared with the control sample. The FT-IR spectroscopic analysis revealed that Zn-Cl stretching in the control and treated sample was at 520 cm^{-1} and 521 cm^{-1}, respectively. The UV-vis analysis exhibited that the wavelength of the maximum absorbance of the control and treated samples was at 196.4 and 196.2 nm, respectively. The TGA thermograms revealed two steps of the thermal degradation and the weight loss of the treated sample was significantly reduced by 22.54% in the 1st step of degradation compared with the control sample. The DSC analysis showed that the enthalpy of decomposition was significantly increased by 34.9% in the treated sample (89.17 J/g) compared with the control sample (66.10 J/g). Overall, DSC and TGA analysis indicated that the thermal stability of the treated sample was increased compared with the control sample. The current study anticipated that The Trivedi Effect®-Energy of Consciousness Healing Treatment might lead to generate a new polymorphic form of zinc chloride, which would be more soluble, stable, and higher absorption rate compared with the control sample. Hence, the treated zinc chloride could be very useful to design the various forms of nutraceuticals and pharmaceutical formulation which might be providing a better

therapeutic response against inflammatory diseases, immunological disorders, aging, stress, cancer, etc.

Keywords: Energy of Consciousness Healing Treatment, Biofield Energy Healing Treatment, Biofield Energy Healers, The Trivedi Effect®, Zinc Chloride, PXRD, Particle Size, Surface Area, TGA, DSC

1. Introduction

Zinc is a vital mineral element in human and animal nutrition with a wide array of biological activities. It plays an important role in catalytic, structural or regulation in greater than 200 zinc metalloenzymes identified in the biological systems [1, 2]. These enzymes are involved in the nucleic acid and protein metabolism as well as for the production of energy. Zinc also maintains the structural integrity of the biological membranes resulting in their protection against oxidative injury [1]. As a metallotherapeutic agent, zinc possesses various pharmacological activities include fertility enhancing, retino-protective, and putative antiviral activities [3]. Zinc is also used in the treatment of Wilson's disease [4]. It also has the immunomodulatory and antioxidant activities [1]. Zinc is also used to prevent the development of several deficiency symptoms include parakeratosis, hypogeusia, anorexia, dysosmia, geophagia, hypogonadism, growth retardation, etc. [5-7]. Recently, it has been reported that zinc had increased the leukocyte count and phagocytic index, which potentiate the immunomodulatory effect along with *Glycyrrhiza glabra* [8]. Zinc chloride ($ZnCl_2$) is hygroscopic inorganic salt and highly soluble in water [9]. It is sometimes used in pharmaceutical industry as drug and diagnostic agent due to its powerful astringent and mild antiseptic properties [10]. It is also used in mouth-wash and deodorant preparations. Zinc chloride is used in as dentin desensitizer *i.e.* reduces the sensitivity of the teeth to heat and cold. The other applications of zinc chloride include protein precipitation and insulin preparation [10, 11]. Literature reported that zinc chloride had been used in the treatment of cancer as a destructive agent [12] and the pluripotency maintenance of mouse embryonic stem cell through the regulation of STAT3 signaling pathway [13]. It can be useful for the palliative treatment of canine and malignant skin wounds [14]. It has opposite effect on the locomotor behavior of rats [15]. Therefore, zinc chloride was considered as one of the components in the novel proprietary herbomineral formulation for the source of zinc ion. This herbomineral formulation is designed as nutraceutical supplement, and can be used for the prevention and treatment of various human disorders.

Every living organism preserves some kind of unique quality, an élan vital or vital force, which contributes the 'life'. From ancient-time this living force is known as prana by the Hindus, *qi* or *chi* by the Chinese, and *ki* by the Japanese and usually is believed to create the source of life that is related with soul, spirit, and mind. Now-a-days, this hypothetical vital force is considered as the Bioenergetics Field. This energy field is a dynamic electromagnetic field existing in the surround of the human body. The Biofield Energy is infinite and paradimensional. It can freely flow between the human and environment that leads to the continuous movement or matter of energy [16, 17]. Thus, the human can harness energy from the earth, the "universal energy field" and transmit it to any living or nonliving object(s) around the globe. The objects always receive the energy and respond in a useful way. This process is known as Biofield Energy Healing Treatment [18, 19]. Biofield (Putative Energy Fields) based Energy Therapies are used worldwide to promote health. The National Center of Complementary and Integrative Health (NCCIH) has been recognized and accepted Biofield Energy Healing as a complementary and alternative medicine (CAM) health care approach in addition to other therapies, medicines and practices such as natural products, deep breathing, yoga, Tai Chi, Qi Gong, chiropractic/osteopathic manipulation, meditation, massage, special diets, homeopathy, progressive relaxation, guided imagery, acupressure, acupuncture, relaxation techniques, hypnotherapy, healing touch, movement therapy, pilates, rolfing structural integration, mindfulness, Ayurvedic medicine, traditional Chinese herbs and medicines, naturopathy, essential oils, aromatherapy, Reiki, cranial sacral therapy and applied prayer (as is common in all religions, like Christianity, Hinduism, Buddhism and Judaism) [20]. Biofield Energy Healing Treatment (The Trivedi Effect®) has been extensively studied with significant outcomes in many scientific fields such as cancer research [21]; altered antimicrobial sensitivity of pathogenic microbes in microbiology [22-24], biotechnology [25, 26], genetics [27, 28]; changing the structure of the atom in relation to various metals, ceramics, polymers and chemicals in materials science [29, 30], altered physical and chemical properties of pharmaceuticals [31, 32], nutraceuticals [33, 34], organic compounds [35-37], and improved overall growth and yield of plants in agricultural science [38, 39]. The physicochemical properties such as particle size, crystalline structure, crystallite size, surface area, etc. and thermal properties of a drug have a vital role in bioavailability as well as the stability of the drug during processing, formulation, storage, and packaging [40, 41]. Biofield Energy Treatment (The Trivedi Effect®) has been reported to change the particle size, specific surface area, crystalline nature, chemical and thermal behavior of an atom/ion through the possible mediation of neutrinos [42]. By considering all these aspects, powder X-ray diffraction (PXRD), particle size distribution analysis (PSD), Fourier transform infrared (FT-IR) spectrometry, ultraviolet-visible (UV-vis) spectroscopy, thermogravimetric analysis (TGA), and differential scanning calorimetry (DSC) analytical techniques were conducted in this study for the characterization of physical, structural, and thermal

properties of the Biofield Energy Treated and untreated zinc chloride.

2. Materials and Methods

2.1. Chemicals and Reagents

Zinc chloride was procured from Tokyo Chemical Industry Co., Ltd. (TCI), Japan. All other chemicals used in the experiment were of analytical grade available in India.

2.2. Biofield Energy Treatment Strategies

Zinc chloride was one of the components of the new proprietary herbomineral formulation, developed by our research team and it was used *per se* as the test compound for the current study. The test compound was divided into two parts, one part of the test compound was treated with The Trivedi Effect® - Energy of Consciousness Healing Treatment (Biofield Energy Treatment) by renowned Biofield Energy Healers and defined as Biofield Energy Treated zinc chloride, while the second part of the test compound did not receive any sort of treatment and defined as untreated or control zinc chloride sample. This Biofield Energy Treatment was provided by the group of eighteen renowned Biofield Energy Healers (The Trivedi Effect®), who participated in this study and performed the Biofield Energy Treatment remotely to the test compound. Eleven Biofield Energy Healers were remotely located in the U.S.A., four remotely located in Canada, one each of the Biofield Energy Healer remotely located in Ireland, United Kingdom, and Russia, performed the Biofield Energy Treatment remotely to the test compound, while the test compound was located in the research laboratory of GVK Biosciences Pvt. Ltd., Hyderabad, India. This Biofield Treatment was provided for 5 minutes through Healer's Unique Energy Transmission process remotely to the test compound under the laboratory conditions. None of the Biofield Energy Healers in this study visited the laboratory in person, nor had any contact with the compounds. Similarly, the control compound was subjected to "sham" healers for 5 minutes, under the same laboratory conditions. The sham healer did not have any knowledge about the Biofield Energy Treatment. After that, the Biofield Energy Treated and the untreated samples were kept in similar sealed conditions and were characterized thoroughly by PXRD, PSD, FT-IR, UV-visible spectroscopy, TGA, and DSC analysis.

2.3. Characterization

2.3.1. Powder X-ray Diffraction (PXRD) Analysis

The PXRD analysis was accomplished on PANalytical X'pert Pro powder X-ray diffractometer system. A total of 500.19 mg for the control and 500.23 mg for the Biofield Energy Treated samples were taken for the analysis. The X-ray of wavelength 1.54056 Å was used. The data were collected in the form of a chart of the Bragg angle (2θ) *vs.* intensity, and a detailed table containing information on peak intensity counts, d value (Å), relative intensity (%), full-width half maximum (FWHM) (θ°). From the XRD results, the crystallite size (G) was calculated using X'pert data collector and X'pert high score plus processing software. The crystallite size (G) was calculated from the Scherrer equation [43, 44]. The method was based on the width of the diffraction patterns obtained in the X-ray reflected the crystalline region. The crystallite size (G) was calculated by using the following equation 1:

$$G = k\lambda/(b\text{Cos}\theta) \quad (1)$$

Where, k is the equipment constant (0.5), λ is the X-ray wavelength (0.154 nm); b in radians is the full-width at half of the peak and θ the corresponding Bragg angle.

Percent change in crystallite size (G) was calculated using the following equation 2:

$$\%\ \text{change in crystallite size} = \frac{[G_{\text{Treated}} - G_{\text{Control}}]}{G_{\text{Control}}} \times 100 \quad (2)$$

Where, $G_{Control}$ and $G_{Treated}$ are the crystallite size of the control and Biofield Energy Treated samples, respectively.

2.3.2. Particle Size Distribution (PSD) Analysis

The average particle size and particle size distribution were analyzed using Malvern Mastersizer 2000, UK with a detection range between 0.01 µm to 3000 µm. The sample unit was filled with dispersant medium and operated the stirrer at 2500 rpm. Alignment of the optics was done and taken the background measurement. After the background measurement, the sample was added to the sample unit with constant monitoring the obscuration and stopped the addition of sample when the obscuration reached in between 15% and 20%. When the obscuration was stable, the measurement was taken twice, and the average was taken of two measurements. The average histogram of the two measurements was recorded. Along with histogram, the data will be presented in the table format which includes particle size (µm). Also, the values at below 10% level (d_{10}), 50% level (d_{50}), and 90% level (d_{90}) were calculated from the histogram, and the calculations such as surface area (m^2/g) were done by using software Mastersizer 2000. Percent change in particle size (d) for at below 10% level (d_{10}), 50% level (d_{50}), and 90% level (d_{90}) was calculated using the following equation 3:

$$\%\ \text{change in particle size} = \frac{[d_{\text{Treated}} - d_{\text{Control}}]}{d_{\text{Control}}} \times 100 \quad (3)$$

Where, $d_{Control}$ and $d_{Treated}$ are the particle size (µm) for at below 10% level (d_{10}), 50% level (d_{50}), and 90% level (d_{90}) of the control and Biofield Energy Treated samples, respectively.

The percent change in surface area (S) was calculated using the following equation 4:

$$\%\ \text{change in surface area} = \frac{[S_{\text{Treated}} - S_{\text{Control}}]}{S_{\text{Control}}} \times 100 \quad (4)$$

Where, $S_{Control}$ and $S_{Treated}$ are the surface area of the control and Biofield Energy Treated samples, respectively.

2.3.3. Fourier Transform Infrared (FT-IR) Spectroscopy

FT-IR spectroscopy of zinc chloride was performed on Spectrum two (Perkin Elmer, USA) Fourier transform infrared spectrometer with the frequency array of 400-4000 cm^{-1} by using pressed KBr disk technique.

2.3.4. Ultraviolet-Visible Spectroscopy (UV-Vis) Analysis

The UV-vis spectroscopic analysis was carried out using Shimadzu UV-2450 with UV Probe, Japan. The spectrum was recorded using 1 cm quartz cell that has a slit width of 1.0 nm. The wavelength ranges chosen for recording the spectra was 190-800 nm. The absorbance spectra (in the range of 0.2 to 0.9) and absorbance maximum (λ_{max}) were recorded.

2.3.5. Thermogravimetric Analysis (TGA)/ Differential Thermogravimetric Analysis (DTG)

The TGA analysis was performed using instruments TGA Q50 (TA instruments, USA) at a heating rate of 10ºC/min from room temperature, *i.e.* 30°C to 900°C under a nitrogen atmosphere (sample mass 16.0260 mg on a platinum pan). In TGA, the weight loss for each step was recorded in grams as well as in a percent loss with respect to the initial weight. Also, the onset, endset, and peak temperature for each step were recorded in TGA. In DTG, the onset, endset, peak temperature and integral area of the peak, change in heat (J/g) of each peak were recorded. Percent change in weight loss (W) was calculated using the following equation 5:

$$\%\ \text{change in weight loss} = \frac{[W_{Treated} - W_{Control}]}{W_{Control}} \times 100 \quad (5)$$

Where, $W_{Control}$ and $W_{Treated}$ are the weight loss of the control and Biofield Energy Treated samples, respectively.

2.3.6. Differential Scanning Calorimetry (DSC)

The analysis was performed using the DSC Q20 (TA instruments, USA) differential scanning calorimeter. Sample quantity of 7.50 mg was weighed and sealed in aluminum pans and equilibrated at 25°C and heated up to 600°C at the heating rate of 10°C/min under nitrogen gas as purge atmosphere with a flow rate of 50 ml/min. The values of onset, endset, peak temperature, peak height (mJ or mW), peak area, and change in heat (J/g) for each peak were recorded. The percent change in melting point (T) was calculated using the following equation 6:

$$\%\ \text{change in melting point} = \frac{[T_{Treated} - T_{Control}]}{T_{Control}} \times 100 \quad (6)$$

Where, $T_{Control}$ and $T_{Treated}$ are the melting point of the control and Biofield Energy Treated samples, respectively.

The percent change in the latent heat of fusion (ΔH) was calculated using the following equation 7:

$$\%\ \text{change in latent heat of fusion} = \frac{[\Delta H_{Treated} - \Delta H_{Control}]}{\Delta H_{Control}} \times 100 \quad (7)$$

Where, $\Delta H_{Control}$ and $\Delta H_{Treated}$ are the latent heat of fusion of the control and Biofield Energy Treated samples, respectively.

3. Results and Discussion

3.1. Powder X-ray Diffraction (PXRD) Analysis

The PXRD diffractograms of both the control and Biofield Energy Treated samples of zinc chloride are shown in Figure 1. The PXRD diffractogram of the control zinc chloride exhibited the intense peaks at Bragg's angle (2θ) equal to 15.87°, 16.82°, 25.68°, 29.58°, 35.19°, 38.50°, 48.91°, 49.44°, 56.41°, 58.54°, and 72.36°. Similarly, the XRD diffractogram of the Biofield Energy Treated zinc chloride exhibited the intense peaks at 2θ equal to 15.87°, 16.82°, 25.69°, 29.62°, 35.18°, 38.51°, 48.91°, 49.42°, 56.47°, 57.68°, and 72.36°. The presence of sharp and intense peaks in the diffractograms revealed that both the samples of zinc chloride are crystalline in nature. The most intense peak was observed at 2θ equal to 49.44° in the control sample and 48.91° in the Biofield Energy Treated sample (Figure 1). It was reported that the alternation in crystal morphology causes the alteration in the relative peak intensities [44].

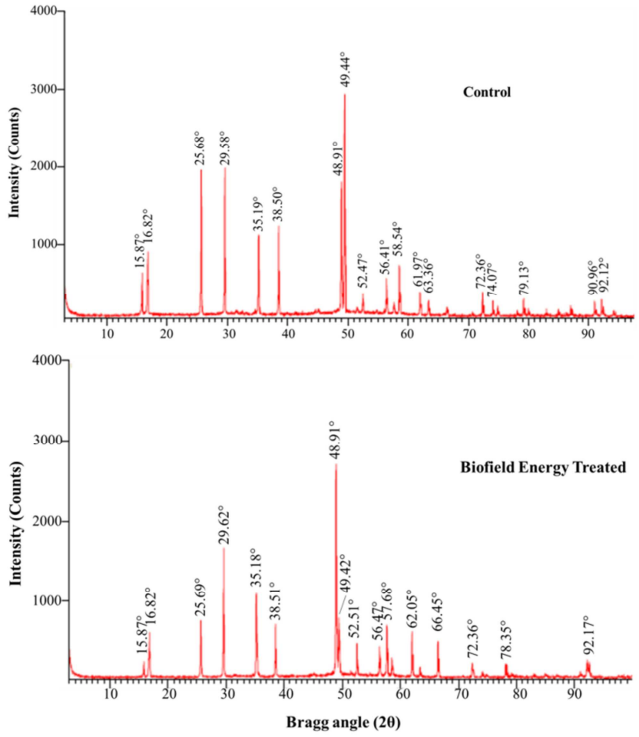

Figure 1. *Powder X-ray diffractograms of the control and Biofield Energy Treated zinc chloride.*

The average crystallite size was calculated using Scherrer equation [43]. The crystallite sizes of the Biofield Energy Treated sample were significantly altered in the range of -49.96 to 50.02% compared with the control sample. The crystallite size of the Biofield Energy Treated zinc chloride at 2θ equal to nearly 25.6°, 56.4°, 58.5°, and 72.3° (Table 1; entry 3, 9, 10, and 11) were significantly decreased in the range of 0.42% to 49.96% compared with the control sample. Consequently, the crystallite size of the Biofield Energy Treated zinc chloride at 2θ equal to 16.8°, 29.6, and 38.5, were increased in the range of 14.28% to 50.2% compared

with the control sample (Table 1; entry 2, 4, and 6). Overall, the crystallite size of the Biofield Energy Treated sodium selenate was decreased by 4.19% compared with the control sample (Table 1). It was reported that increased in lattice strain may reduce the crystallite size of the sample [45]. Therefore, it is hypothesized that Biofield Energy may induce some lattice strain within the treated molecules of zinc chloride. As a result, the grains were fractured into sub-grains that could lead to decrease the crystallite size of the Biofield Energy Treated sample compared with the control sample. The study revealed that the Biofield Energy Treatment might be introduced a new polymorphic form of zinc chloride [46]. The decrease in crystallite size of the Biofield Energy Treated zinc chloride might increase its surface area and solubility compared with the control sample.

Table 1. *PXRD data for the control and Biofield Energy Treated zinc chloride.*

Entry No.	Bragg angle (°2θ)		Relative Intensity (%)		FWHM (°2θ)		Crystallite size (G, nm)		
	Control	Treated	Control	Treated	Control	Treated	Control	Treated	% change[a]
1	15.87	15.87	21.91	8.77	0.1004	0.1004	44.27	44.27	0.00
2	16.82	16.82	34.48	21.62	0.2007	0.1338	22.17	33.26	50.02
3	25.68	25.69	79.18	27.85	0.1171	0.1338	38.56	33.75	-12.47
4	29.58	29.62	67.94	71.45	0.1338	0.1171	34.03	38.89	14.28
5	35.19	35.18	40.91	42.54	0.1338	0.1338	34.52	34.52	0.00
6	38.50	38.51	43.10	27.17	0.1673	0.1338	27.88	34.86	25.04
7	48.91	48.91	58.81	100.00	0.1338	0.1338	36.16	36.16	0.00
8	49.44	49.42	100.00	31.77	0.1004	0.1004	48.29	48.29	0.00
9	56.41	56.47	16.78	9.30	0.1004	0.2007	49.78	24.91	-49.96
10	58.54	57.68	24.25	10.22	0.1004	0.1004	50.30	50.09	-0.42
11	72.36	72.36	12.51	7.83	0.1224	0.1632	44.61	33.46	-24.99
12	Average crystallite size						39.14	37.50	-4.19

FMHM: Full width at half maximum, [a] denotes the percentage in the crystallite size of the Biofield Energy Treated sample with respect to the control sample.

3.2. Particle Size Distribution (PSD) Analysis

Particle sizes ($d_{10,}$ $d_{50,}$ and d_{90}) of the control and Biofield Energy Treated zinc chloride were investigated, and the results are presented in Table 2. The particle size at d_{10} and d_{50} values of the Biofield Energy Treated sample decreased by 4.72% and 2.70%, respectively compared with the control sample. But, the particle size of the Biofield Energy Treated sample increased at d_{90} by 0.83% compared with the control sample. The control sample showed a surface area of 3.11 m^2/g and it was increased to 3.21 m^2/g in the Biofield Energy Treated zinc chloride (Table 2). Thus, the surface area of the Biofield Energy Treated sample was increased by 3.22% compared with the control sample. The results revealed that there might be an effect of high energy milling induced through the Biofield Energy Treatment to zinc chloride. Surface area has a major influence on the dissolution of a particle in a solvent. The reason that surface energy is the driving factor for dissolution efficiency and it is mainly influenced by the surface area and chemical affinity. The reduction in the particle size and increase in the surface area has a significant impact on the increase in dissolution, release, absorption, drug action, and dose uniformity of pharmaceuticals/nutraceuticals in various drug delivery system [47].

Table 2. *Particle size data ($d_{10,}$ d_{50} and d_{90}) and surface area of the control and Biofield Energy Treated zinc chloride.*

Test Item	d_{10} (µm)	d_{50} (µm)	d_{90} (µm)	Surface area (m^2/g)
Zinc chloride (Control)	0.974	2.560	5.912	3.11
Zinc chloride (Biofield Treated)	0.928	2.491	5.961	3.21
Percent change[a] (%)	-4.72	-2.70	0.83	3.22

[a] denotes the percentage change in the particle size data ($d_{10,}$ $d_{50,}$ and d_{90}) and surface area of the Biofield Energy Treated sample with respect to the control sample.

3.3. Fourier Transform Infrared (FT-IR) Spectroscopy

The FT-IR spectra of both the control and Biofield Energy Treated zinc chloride are presented in Figure 2. Zinc chloride is a tri-atomic molecule that shows SP hybridization with a bond angle of 180°, which is linear with four numbers of normal modes of vibration. The FT-IR spectra showed the O-H stretching at 3900 cm^{-1} in both the control and Biofield Energy Treated samples [48]. The peak might be because of the hydrates of zinc chloride $\{ZnCl_2(H_2O)_n$ where n = 1, 1.5, 2.5, 3, and 4} [48]. The metal halides (*i.e.* Zn-Cl) show IR peak in the range of 750-100 cm^{-1} [49, 50]. The Zn-Cl stretching of the control and Biofield Energy Treated samples was found at 520 cm^{-1} and 521 cm^{-1}, respectively. Overall, IR peaks of the Biofield Energy Treated zinc chloride did not show any significant structural changes with respect to the control sample.

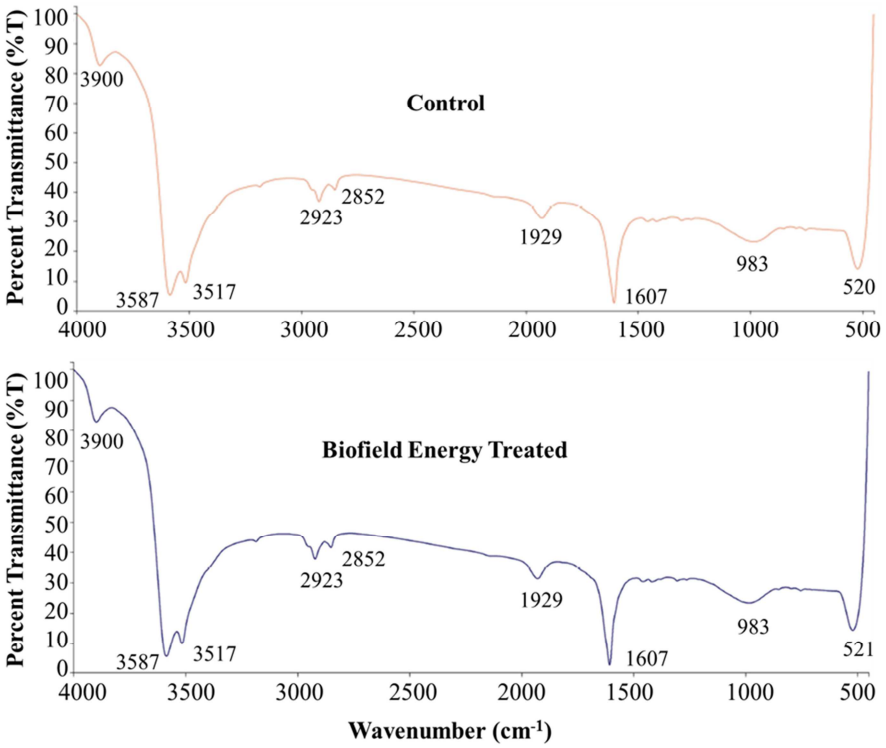

Figure 2. *FT-IR spectra of the control and Biofield Energy Treated zinc chloride.*

3.4. Ultraviolet-Visible Spectroscopy (UV-Vis) Analysis

The UV-visible spectra of both the control and Biofield Energy Treated zinc chloride are shown in Figure 3. The control and Biofield Energy Treated sample exhibited the wavelength of maximum absorbance (λ_{max}) at 196.4 and 196.2 nm, respectively. The peak at 196 nm was indicated a minor shift of absorbance maxima from 1.9793 (control) to 1.9042 (the Biofield Energy Treated sample). It was reported that the UV absorbance occurred due to excitation of electrons from the highest energy occupied molecular orbital (HOMO) to the lowest energy unoccupied molecular orbital (LUMO) [32, 51]. However, the UV analysis of zinc chloride showed no change in the λ_{max} of the Biofield Energy Treated sample compared with the control sample. It indicated that energy gap between the HOMO and LUMO in the Biofield Energy Treated zinc chloride was comparatively similar to that of the control sample.

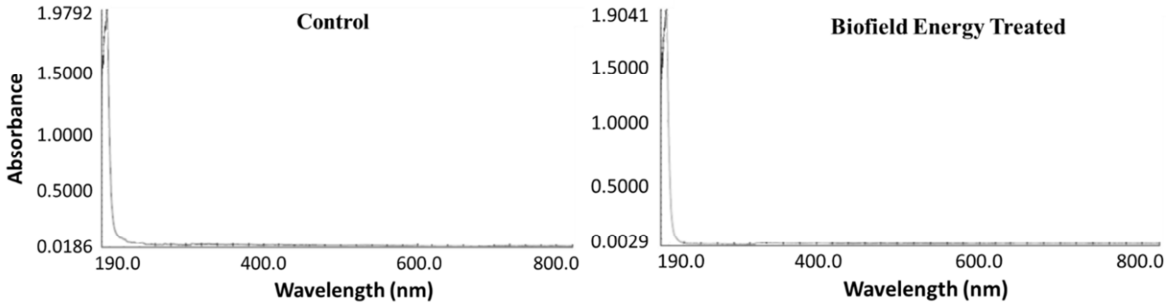

Figure 3. *UV-Vis spectra of the control and Biofield Energy Treated zinc chloride.*

3.5. Thermogravimetric Analysis (TGA)/ Differential Thermogravimetric Analysis (DTG)

The TGA and DTG thermograms of the control and Biofield Energy Treated samples are shown in Figures 4 and 5 respectively, which showed two steps of the thermal degradation process (Table 3). The TGA thermograms revealed that the weight loss of the Biofield Energy Treated sample was significantly reduced by 22.54% in the 1st step of degradation compared with the control sample. Unlikely, the weight loss of the Biofield Energy Treated sample was slightly increased by 0.64% in the 2st step of degradation compared with the control sample. The pattern of thermal degradation of the control zinc chloride was nearly matched with the reported data [52]. The control and Biofield Energy Treated samples had lost their weight by 98.63% and 98.13%, respectively from their total original weight during

the process. The total weight loss was decreased in the Biofield Energy Treated zinc chloride by 0.51% compared with the control sample. The DTG thermograms (Figure 5) exhibited two peaks in both the samples. The DTG thermograms of the control and Biofield Energy Treated samples disclosed the maximum temperature (T_{max}) at 505.60°C and 501.24°C, respectively. The DTG analysis indicated that the decomposition temperature of the Biofield Energy Treated zinc chloride was slightly lower (0.86%) than the control sample.

The overall results concluded that the thermal stability of the Biofield Energy Treated zinc chloride was increased compared with the control sample. The improvement in the thermal stability would be the advantage in the long term storage stability and shelf-life of the nutraceutical/pharmaceutical products [53].

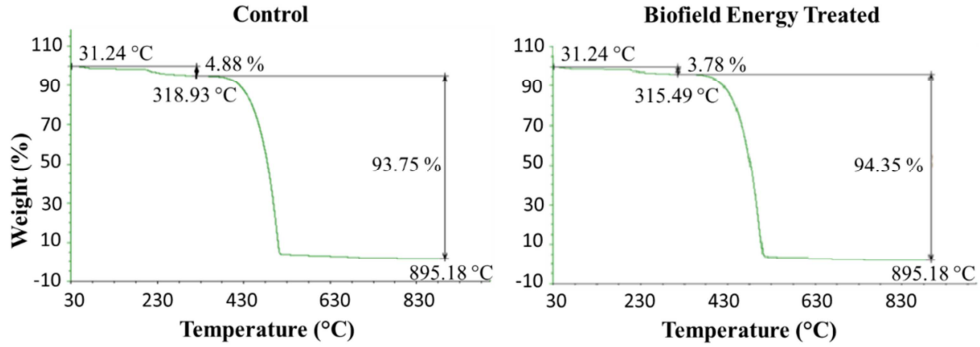

Figure 4. *The TGA thermograms of control and Biofield Energy Treated zinc chloride.*

Table 3. *Thermal degradation data of the control and Biofield Energy Treated zinc chloride.*

S. No.	Temperature (°C)		% Weight loss		% Change[a]
	Control	Treated	Control	Treated	
1st step of degradation	318.93	315.49	4.88	3.78	-22.54
2nd step of degradation	895.18	895.18	93.75	94.35	0.64
Total weight loss	-	-	98.63	98.13	-0.51

[a] denotes the percentage change in the weight loss of the Biofield Energy Treated sample with respect to the control sample.

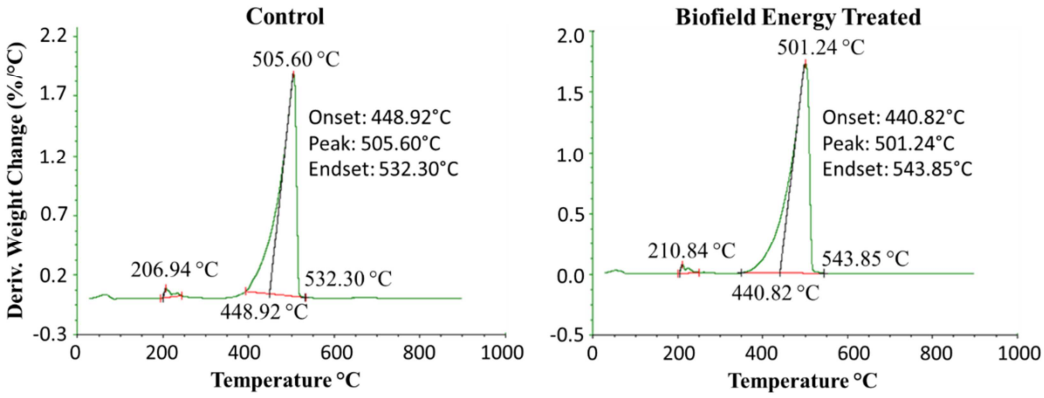

Figure 5. *DTG thermograms of the control and Biofield Energy Treated zinc chloride.*

3.6. Differential Scanning Calorimetry (DSC) Analysis

Measurement of the decomposition temperature and enthalpy of decomposition of the control and Biofield Energy Treated samples of zinc chloride was performed using DSC analysis, and the results are presented in Figure 6 and Table 4. The DSC thermograms of the control and Biofield Energy Treated samples represented the sharp exothermic peak in both the samples. The enthalpy of decomposition (ΔH) was increased by 34.9% in the Biofield Energy Treated sample (66.10 J/g) compared with the control sample (89.17 J/g). A slight lowering decomposition temperature by 2.12% was observed in the Biofield Energy Treated zinc chloride (439.81°C) compared with the control sample (449.32°C). The results suggested it can be hypothesized that the Biofield Energy Treatment might cause some alteration in kinetic energy of the Biofield Energy Treated sample compared with the control. Thus, the Biofield Energy Treated zinc chloride needs more energy in the form of enthalpy of decomposition to undergo the process of decomposition compared with the control sample. The intermolecular force possibly increased the enthalpy of decomposition due to the Biofield Energy Treatment. The enhanced thermal stability of a drug is an advantage in the maintenance of the product in long term storage condition throughout the shelf-life for any pharmaceutical formulations [54].

Table 4. *The enthalpy of decomposition (J/G) and degradation temperature (°C) of the control and Biofield Energy Treated zinc chloride.*

Sample	Enthalpy of decomposition (ΔH) J/g	Onset decomposition temperature (T_{onset})°C	Peak decomposition temperature (T_{peak})°C	Endset decomposition temperature (T_{endset})°C
Control	66.10	443.07	449.32	452.86
Biofield Energy Treated	89.17	433.29	439.81	442.56
% Change[a]	34.90	-2.21	-2.12	-2.27

T_{onset}: Onset melting temperature, T_{peak}: Peak decomposition temperature, T_{endset}: Endset decomposition temperature, ΔH: Enthalpy of decomposition, [a] denotes the percentage change of the Biofield Energy Treated sample with respect to the control sample.

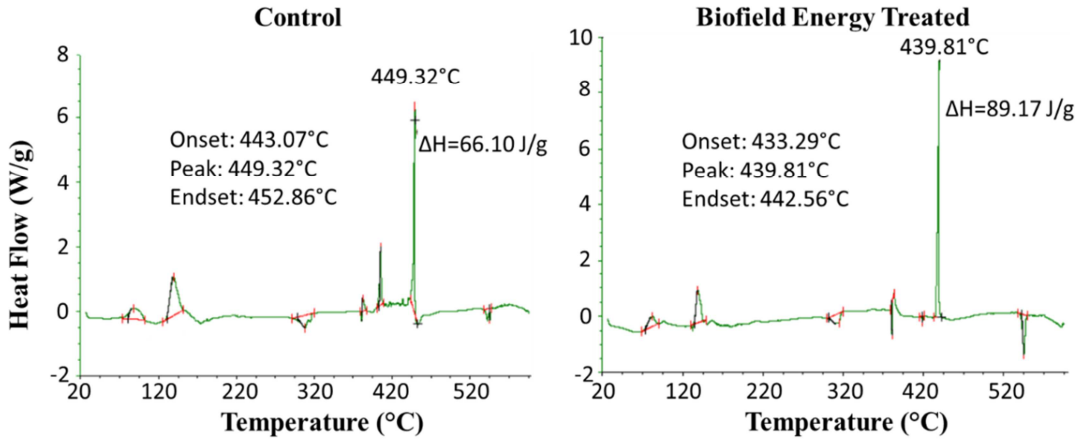

Figure 6. *DSC thermograms of the control and Biofield Energy Treated zinc chloride.*

4. Conclusions

The current study revealed that the Consciousness Energy Healing Treatment (The Trivedi Effect®) had the notable effects on the physicochemical and thermal properties of zinc chloride. A significant change of the crystallite size and relative intensities of the PXRD peaks was observed in the treated sample compared with the control sample. The crystallite sizes of the treated sample were significantly altered in the range of -49.96% to 50.02% compared with the control sample. The crystallite size of the treated sample was decreased by 4.19% compared with the control sample. The particle size values of the Biofield Energy Treated sample at d_{10} and d_{50} were decreased by 4.72% and 2.70%, respectively whereas, at d_{90} it was increased by 0.83% compared with the control sample. Consequently, the surface area was increased by 3.22% in the treated sample compared with the control sample. The FT-IR spectroscopic analysis revealed that Zn-Cl stretching in the control and treated sample was at 520 cm^{-1} and 521 cm^{-1}, respectively. The UV-vis analysis exhibited that the wavelength of the maximum absorbance (λ_{max}) of the control and treated samples was at 196.4 and 196.2 nm, respectively. The TGA thermograms revealed two steps of thermal degradation and the weight loss of the treated sample was significantly reduced by 22.54% in the 1st step of degradation compared with the control sample. The DSC analysis showed that the enthalpy of decomposition was significantly increased by 34.9% in the treated sample (ΔH = 89.17 J/g) compared with the control sample (ΔH = 66.10 J/g). Overall, DSC and TGA analysis indicated that the thermal stability of the treated sample was increased compared with the control sample. The current study anticipated that The Trivedi Effect®-Energy of Consciousness Healing Treatment might lead to generate a new polymorphic form of zinc chloride, which would be more soluble, stable, and higher absorption rate compared with the control sample. Hence, the treated zinc chloride could be very useful to design the various forms of nutraceuticals and/or pharmaceutical formulation that might offer a better therapeutic response against inflammatory diseases, immunological disorders, aging, stress, Wilson's disease, viral diseases, parakeratosis, hypogeusia, anorexia, dysosmia, geophagia, hypogonadism, growth retardation, etc.

Abbreviations

DSC: Differential scanning calorimetry, FT-IR: Fourier transform infrared, FWHM: Full width half maximum, ΔH: Enthalpy of decomposition, HOMO: Highest energy occupied molecular orbital, LUMO: Lowest energy unoccupied molecular orbital, PSD: Particle size distribution, T_{onset}: Onset decomposition temperature, T_{peak}: Peak decomposition temperature, T_{endset}: Endset decomposition temperature, TGA: Thermogravimetric analysis, UV-vis: Ultra-violet Visible spectroscopy, PXRD: Powder X-ray diffraction.

Acknowledgements

The authors are grateful to GVK Biosciences Pvt. Ltd., Hyderabad, India, Trivedi Science, Trivedi Global, Inc., and Trivedi Master Wellness for their support throughout the work.

References

[1] Ronconi L, Sadler PJ (2008) Applications of heteronuclear NMR spectroscopy in biological and medicinal inorganic chemistry. Coordn Chem Rev 252: 2239-2277.

[2] Berg JM, Shi Y (1996) The galvanization of biology: A growing appreciation for the roles of zinc. Science 271: 1081-1085.

[3] Higdon JV, Ho E (2005) In: M. Gielen, E.R.T. Tiekink (Eds.), Metallotherapeutic drugs and metal-based diagnostic agents: The use of metals in medicine, Wiley-VCH, Weinheim, p. 237.

[4] *Brewer GJ (2001) Zinc acetate for the treatment of Wilson's disease. Expert Opin Pharmacother 2: 1473-1477.*

[5] Prasad AS (1979) Clinical, biochemical, and pharmacological role of zinc. Ann Rev Pharmacol Toxicol 19: 393-426.

[6] Supuran CT (2008) Carbonic anhydrases: Novel therapeutic applications for inhibitors and activators. Nat Rev Drug Dis 7: 168-181.

[7] Elmes ME (1975) Letter: Zinc in human medicine. Lancet 2: 549.

[8] Mazumder PM, Pattnayak S, Parvani H, Sasmal D, Rathinavelusamy P (2012) Evaluation of immunomodulatory activity of *Glycyrhiza glabra* L. roots in combination with zing. Asian Pac J Trop Biomed 2: S15-S20.

[9] Brynestad J, Yakel HL (1978) Preparation and structure of anhydrous zinc chloride. Inorg Chem 17: 1376-1377.

[10] Kasture AV, Wadodkar SG (2008) A text book of pharmaceutical chemistry-1, Nirali Prakashan, 25th Ed., Pune, India.

[11] Mahadik KR, Kuchekar BS (2008) Concise inorganic pharmaceutical chemistry, Nirali Prakashan, 25th Ed., Pune, India.

[12] *McDaniel S, Goldman GD (2002) Consequences of using escharotic agents as primary treatment for nonmelanoma skin cancer. Arch Dermatol 138: 1593-1596.*

[13] Hu J, Yang Z, Wang J, Yu J, Guo J, Liu S, Qian C, Song L, Wu Y, Cheng J (2016) Zinc chloride transiently maintains mouse embryonic stem cell pluripotency by activating Stat3 signaling. PLoS One 11: e0148994.

[14] Fukuyama Y, Kawarai S, Tezuka T, Kawabata A, Maruo T (2016) The palliative efficacy of modified Mohs paste for controlling canine and feline malignant skin wounds. Vet Q 1: 1-7.

[15] Yakimovskii AF, Kryzhanovskaya SY (2015) Zinc chloride and zinc acetate injected into the neostriatum produce opposite effect on locomotor behavior of rats. Bull Exp Biol Med 160: 281-282.

[16] Stenger VJ (1999) Bioenergetic fields. Sci Rev Alternative Med 3: 16-21.

[17] Rogers, M (1989) "Nursing: A Science of Unitary Human Beings." In J.P. Riehl-Sisca (ed.) Conceptual Models for Nursing Practice. 3rd Edn. Norwark: Appleton & Lange.

[18] Rosa L, Rosa E, Sarner L, Barrett S (1998) A close look at therapeutic touch. Journal of the American Medical Association 279: 1005-1010.

[19] Warber SL, Cornelio D, Straughn, J, Kile G (2004) Biofield energy healing from the inside. J Altern Complement Med 10: 1107-1113.

[20] Koithan M (2009) Introducing complementary and alternative therapies. J Nurse Pract 5: 18-20.

[21] Trivedi MK, Patil S, Shettigar H, Mondal SC, Jana S (2015) The potential impact of biofield treatment on human brain tumor cells: A time-lapse video microscopy. J Integr Oncol 4: 141.

[22] Trivedi MK, Patil S, Shettigar H, Gangwar M, Jana S (2015) An evaluation of biofield treatment on susceptibility pattern of multidrug resistant *Stenotrophomonas maltophilia*: An emerging global opportunistic pathogen. Clin Microbiol 4: 211.

[23] Trivedi MK, Patil S, Shettigar H, Gangwar M, Jana S (2015) An effect of biofield treatment on multidrug-resistant *Burkholderia cepacia*: A multihost pathogen. J Trop Dis 3: 167.

[24] Trivedi MK, Patil S, Shettigar H, Bairwa K, Jana S (2015) Phenotypic and biotypic characterization of *Klebsiella oxytoca*: An impact of biofield treatment. J Microb Biochem Technol 7: 203-206.

[25] Trivedi MK, Branton A, Trivedi D, Nayak G, Mondal SC, Jana S (2015) Antibiogram, biochemical reactions and genotyping characterization of biofield treated *Staphylococcus aureus*. American Journal of BioScience 3: 212-220.

[26] Trivedi MK, Branton A, Trivedi D, Nayak G, Bairwa K, Jana S (2015) Physical, thermal, and spectroscopic characterization of biofield energy treated potato micropropagation medium. American Journal of Bioscience and Bioengineering 3: 106-113.

[27] Trivedi MK, Branton A, Trivedi D, Nayak G, Mondal SC, Jana S (2015) Biochemical differentiation and molecular characterization of biofield treated *Vibrio parahaemolyticus*. American Journal of Clinical and Experimental Medicine 3: 260-267.

[28] Trivedi MK, Branton A, Trivedi D, Gangwar M, Jana S (2015) Antimicrobial susceptibility, biochemical characterization and molecular typing of biofield treated *Klebsiella pneumoniae*. J Health Med Inform 6: 206.

[29] Trivedi MK, Tallapragada RM, Branton A, Trivedi D, Nayak G, Latiyal O, Jana S (2015) Analysis of physical, thermal, and structural properties of biofield energy treated molybdenum dioxide. International Journal of Materials Science and Applications 4: 354-359.

[30] Trivedi MK, Tallapragada RM, Branton A, Trivedi D, Nayak G, Latiyal O, Jana S (2015) Characterization of atomic and physical properties of biofield energy treated manganese sulfide powder. American Journal of Physics and Applications 3: 215-220.

[31] Trivedi MK, Branton A, Trivedi D, Nayak G, Saikia G, Jana S (2015) Physical and structural characterization of biofield treated imidazole derivatives. Nat Prod Chem Res 3: 187.

[32] Trivedi MK, Tallapragada RM, Branton A, Trivedi D, Nayak G, Mishra RK, Jana S (2015) Characterization of physical, spectral and thermal properties of biofield treated 1,2,4-Triazole. J Mol Pharm Org Process Res 3: 128.

[33] Trivedi MK, Tallapragada RM, Branton A, Trivedi D, Nayak G, Mishra RK, Jana S (2015) Biofield treatment: A potential strategy for modification of physical and thermal properties of gluten hydrolysate and ipomoea macroelements. J Nutr Food Sci 5: 414.

[34] Trivedi MK, Nayak G, Patil S, Tallapragada RM, Jana S, Mishra RK (2015) Bio-field Treatment: An effective strategy to improve the quality of beef extract and meat infusion powder. J Nutr Food Sci 5: 389.

[35] Trivedi MK, Branton A, Trivedi D, Nayak G, Latiyal O, Jana S (2015) Evaluation of biofield treatment on atomic and thermal properties of ethanol. Organic Chem Curr Res 4: 145.

[36] Trivedi MK, Branton A, Trivedi D, Nayak G, Singh R, Jana S (2015) Physical, thermal and spectroscopic studies on biofield treated *p*-dichlorobenzene. Biochem Anal Biochem 4: 204.

[37] Trivedi MK, Branton A, Trivedi D, Nayak G, Bairwa K, Jana S (2015) Physicochemical and spectroscopic characterization of biofield energy treated *p*-anisidine. Pharm Anal Chem Open Access 6: 102.

[38] Trivedi MK, Branton A, Trivedi D, Nayak G, Gangwar M, Jana S (2015) Agronomic characteristics, growth analysis, and yield response of biofield treated mustard, cowpea, horse gram, and groundnuts. International Journal of Genetics and Genomics 3: 74-80.

[39] Trivedi MK, Branton A, Trivedi D, Nayak G, Gangwar M, Jana S (2015) Analysis of genetic diversity using simple sequence repeat (SSR) markers and growth regulator response in biofield treated cotton (*Gossypium hirsutum* L.). American Journal of Agriculture and Forestry 3: 216-221.

[40] Chereson R (2009) Bioavailability, bioequivalence, and drug selection. In: Makoid CM, Vuchetich PJ, Banakar UV (Eds) Basic pharmacokinetics (1st Edn) Pharmaceutical Press, London.

[41] Blagden N, de Matas M, Gavan PT, York P (2007) Crystal engineering of active pharmaceutical ingredients to improve solubility and dissolution rates. Adv Drug Deliv Rev 59: 617-630.

[42] Trivedi MK, Mohan TRR (2016) Biofield energy signals, energy transmission and neutrinos. American Journal of Modern Physics 5: 172-176.

[43] Langford JI, Wilson AJC (1978) Scherrer after sixty years: a survey and some new results in the determination of crystallite size. J Appl Cryst 11: 102-113.

[44] Inoue M, Hirasawa I (2013) The relationship between crystal morphology and XRD peak intensity on $CaSO_4.2H_2O$. J Crystal Growth 380: 169-175.

[45] Balzar D, Audebrand N, Daymond MR, Fitch A, Hewat A, Langford JI, Le Bail A, Louër D, Masson O, McCowan CN, Popa NC, Stephens PW, Toby BH (2004) Size-strain line-broadening analysis of the ceria round-robin sample. J Appl Cryst 37: 911-924.

[46] Raza K, Kumar P, Ratan S, Malik R, Arora S (2014) Polymorphism: The phenomenon affecting the performance of drugs. SOJ Pharm Pharm Sci 1: 10.

[47] Martin AN, Patrick JS (2006) Martin's physical pharmacy and pharmaceutical sciences: physical chemical and biopharmaceutical principles in the pharmaceutical sciences. Phila: Lippincott Williams and Wilkins.

[48] Coates J (2000) Interpretation of Infrared Spectra, A practical approach in encyclopedia of analytical chemistry. John Wiley & Sons Ltd, Chichester.

[49] Holleman AF, Wiberg E (2001) Inorganic chemistry. San Diego: Academic Press.

[50] Prasanna D, Premkumar B, Kumaresan S (2014) Synthesis, growth and characterization of pure and magnesium doped triglycine zinc chloride single crystals. Int J Chem Tech Res 6: 1643-1646.

[51] Hesse M, Meier H, Zeeh B (1997) Spectroscopic methods in organic chemistry, Georg Thieme Verlag Stuttgart, New York.

[52] Martin FJ, Albers H, Lambeck PV, Van de Velde GMH, Popma ThJA (1991) Luminescent thin films by the chemical aerosol deposition technology (CADT). Aerosol Sci 22: S435-S438.

[53] Bajaj S, Singla D, Sakhuja N (2012) Stability testing of pharmaceutical products. J App Pharm Sci 2: 129-138.

[54] Troy DB, Beringer P (2006) Remington: The science and practice of pharmacy: Instrumental method of analysis. 21st Edition, Chapter 34.